Decomposition of POLSAR Image Applied to Wet Land Monitoring

Yoshio Yamaguchi[1], Yuki Yajima[1], Ryoichi Sato[2], Hiroyoshi Yamada[1], Wolfgang –M. Boerner[3]
[1] *Faculty of Engineering,* [2] *Faculty of Education, Niigata University*
Ikarashi 2-8050, Niigata, 950-2181 Japan
yamaguch@ie.niigata-u.ac.jp
[3] *University of Illinois at Chicago, USA*

Abstract

A scheme for four-component scattering power decomposition has been developed for polarimetric SAR image analysis based on the coherency matrix. The four-component consists of surface scattering, double bounce scattering, volume scattering, and helix scattering power. This decomposition scheme is applied to the L- and X-band polarimetric data acquired by the airborne Pi-SAR system and is used to monitor seasonal change of wetland area, a lake "SAKATA" in Niigata, Japan. It is shown that the four-component powers represent typical seasonal feature of vegetation near by the lake.

1. INTRODUCTION

Terrain and land use classification is one of the most important applications of Polarimetric Synthetic Aperture Radar (POLSAR) sensing. POLSAR acquires scattering matrix over land. Based on the second order statistics of scattering nature, namely, on the coherency matrix and/or covariance matrix, a four component scattering power decomposition method has been proposed [1]-[2], which deals with general scattering case. This scheme has advantages such that the decomposed power can be expressed in terms of scattering elements directly, which, in turn, is suitable for direct physical interpretation of data and phenomena, easy calculation and implementation. This scheme is applied to monitor seasonal change of wetland area. The site is located in Niigata Prefecture where a small lake named "SAKATA" is registered for Convention on Wetlands of International Importance especially as Waterfowl Habitat (Ramsar Treaty). In this paper, the decomposition scheme and the decomposed results are presented.

2. DECOMPOSITION OF POLSAR DATA

For simplicity, we write the scattering matrix as

$$[\,S\,(HV)\,] = \begin{bmatrix} S_{HH} & S_{HV} \\ S_{VH} & S_{VV} \end{bmatrix} = \begin{bmatrix} a & c \\ c & b \end{bmatrix} \qquad (1)$$

assuming the backscattering case $S_{HV} = S_{VH} = c$. The ensemble average coherency matrix is given as

$$\langle [\,T\,] \rangle = \frac{1}{2} \begin{bmatrix} \langle |a+b|^2 \rangle & \langle (a+b)(a \Phi b)^* \rangle & \langle 2(a+b)\,c^* \rangle \\ \langle (a \Phi b)(a+b)^* \rangle & \langle |a \Phi b|^2 \rangle & \langle 2(a \Phi b)\,c^* \rangle \\ \langle 2c\,(a+b)^* \rangle & \langle 2c\,(a \Phi b)^* \rangle & \langle 4\,|c|^2 \rangle \end{bmatrix} \qquad (2)$$

The advantages of coherency matrix are mathematical orthogonality and representation of scattering mechanism for ideal target. We expand the measured coherency into four scattering matrices as

$$\langle [\,T\,] \rangle = f_s [\,T\,]_{surface} + f_d [\,T\,]_{double} + f_v \langle [\,T\,] \rangle_{vol} + f_c \langle [\,T\,] \rangle_{helix} \qquad (3)$$

where f_s, f_d, f_v, *and* f_c are the expansion coefficients. The expansion matrices are based on scattering mechanisms as shown in Fig.1 and can be constructed as follows:

Fig. 1 Four-component scattering model

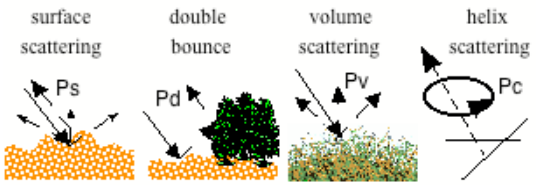

The surface scattering model

$$[\,T\,]_{surface} = \begin{bmatrix} 1 & \in^* & 0 \\ \in & |\in|^2 & 0 \\ 0 & 0 & 0 \end{bmatrix}, \quad |\in| < 1 \qquad (4)$$

The double bounce scattering model,

$$[\,T\,]_{double} = \begin{bmatrix} |\nearrow|^2 & \nearrow & 0 \\ \nearrow^* & 1 & 0 \\ 0 & 0 & 0 \end{bmatrix}, \quad |\nearrow| < 1 \qquad (5)$$

$\nearrow$ and $\in$ are unknowns to be determined.

The volume scattering model,

$$\langle [\ T\ ] \rangle_{vol} = \frac{1}{4} \begin{bmatrix} 2 & 0 & 0 \\ 0 & 1 & 0 \\ 0 & 0 & 1 \end{bmatrix} \tag{6}$$

The Helix scattering model,

$$\langle [\ T\ ] \rangle_{helix} = \frac{1}{2} \begin{bmatrix} 0 & 0 & 0 \\ 0 & 1 & \pm j \\ 0 & \mp j & 1 \end{bmatrix} \tag{7}$$

By equating the measured data to the expansion matrices (3) we can obtain the unknowns. Since the trace of coherency matrix yields the corresponding scattering power, the following four-component scattering powers can be derived.

Helix scattering power (circular polarization power) : Pc

$$P_c = f_c = 2 \mid \mathrm{Im} \langle c^* (a \Phi b) \rangle \mid \tag{8}$$

The volume scattering power : *Pv*

$$P_v = f_v = 8 \left\langle |c|^2 \right\rangle \Phi 2\ P_c \ . \tag{9}$$

Since the number of unknowns exceeds the number of equations, we need an assumption to determine the remaining surface scattering power Ps and double scattering power Pd. Since the sign of $\mathrm{Re} \left\langle S_{HH} S_{VV}^* \right\rangle$ plays an important role for discriminating them physically, we incorporate it in this criterion

$$C_0 = \langle a\, b^* \rangle - \langle |c|^2 \rangle + \frac{1}{2} P_c \,. \tag{10}$$

$$\text{If } \mathrm{Re}\{C_0\} > 0, \text{ then } P_s = S - \frac{|C|^2}{D} \text{ and } P_d = D + \frac{|C|^2}{D}$$

$$\text{If } \mathrm{Re}\{C_0\} < 0, \text{ then } P_s = S + \frac{|C|^2}{S} \text{ and } P_d = D - \frac{|C|^2}{S} \tag{11}$$

where *S, D*, and *C* are given by

$$S = \frac{1}{2} \left\langle |a + b|^2 \right\rangle \Phi 4 \left\langle |c|^2 \right\rangle + P_c \tag{12a}$$

$$D = \frac{1}{2} \left\langle |a \Phi b|^2 \right\rangle \Phi 2 \left\langle |c|^2 \right\rangle \tag{12b}$$

$$C = \frac{1}{2} \left\langle (a + b)(a \Phi b)^* \right\rangle . \tag{13c}$$

It should be noted that enforcing Pc=0 in the above equations result in the three-component decomposition [3]. Therefore this four-component decomposition is natural extension of 3-component decomposition.

3. PI-SAR OBSERVATION

Pi-SAR is an airborne Polarimetric interferometric Synthetic Aperture Radar system developed by NiCT and JAXA, Japan. It has dual frequency (L- and X-) band and fully polarimetric data take function mode. The resolution on the ground is 1.5 by 1.5 m in the X band and 3 by 3 m in the L band. It has flown over Niigata area several times. The detailed information is listed in Table 1.

Table 1: Pi-SAR data description

Mode	Quad. Pol.	HH+HV+ VH+ VV
Date	2004/2/4	Incidence angle: 31.71-46.13 [deg]
	2004/8/4	Incidence angle: 30.19-44.18 [deg]
	2004/11/3	Incidence angle: 31.19-45.49 [deg]
L-band	1.27 GHz	2000 by 2000 pixels
Pixel size: 2.5 by 2.5 m		Averaging size: 5 by 5 pixels
X-band	9.55 GHz	4000 by 4000 pixels
Pixel size: 1.25 by 1.25 m		Averaging size: 10 by10 pixels

The test area is "SAKATA" in Niigata Prefecture, Japan. The picture is shown in Fig.2. In the middle of the small lake, lotus grows in summer season. The rim of the lake is surrounded by Reed. The water level changes season by season. This area is registered for Ramsar Treaty on Wetlands of International Importance especially as Waterfowl Habitat such as for migrating birds. It is interesting to investigate the seasonal environments on these preserved area.

(a) overview

(b) Lotus

(c) Reeds

Fig. 2 SAKATA lake, Niigata, Japan

4. POLSAR DATA ANALYSIS

Four-component decomposition scheme was applied to the acquired data by Pi-SAR. Fig.3 shows the decomposed results.

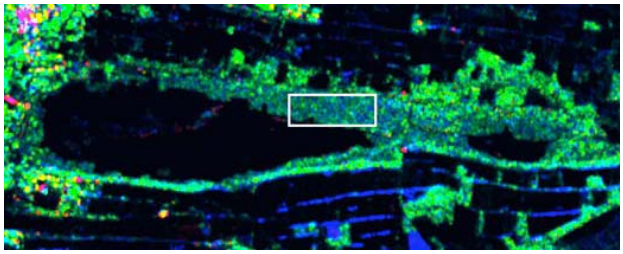

(a) L-band decomposed image in 2004.2

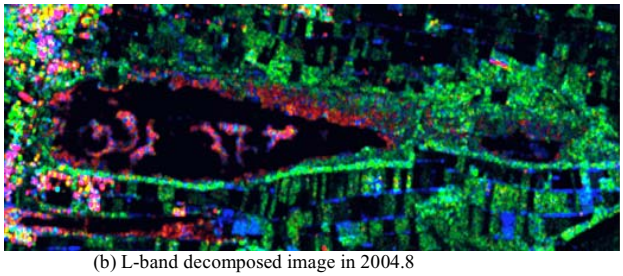

(b) L-band decomposed image in 2004.8

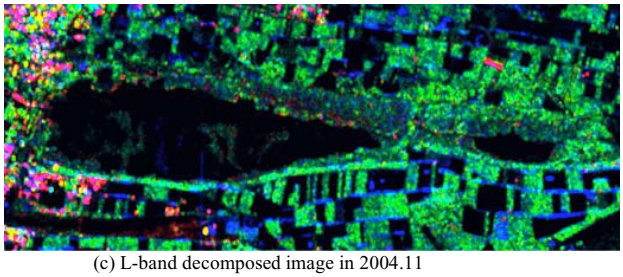

(c) L-band decomposed image in 2004.11

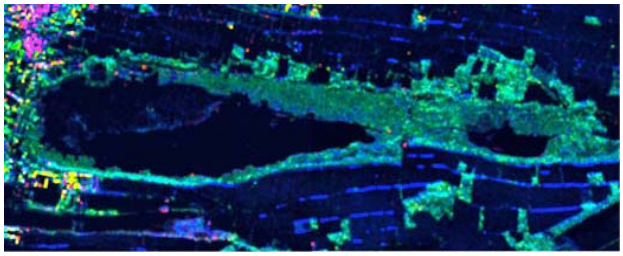

(d) X-band decomposed image in 2004.2

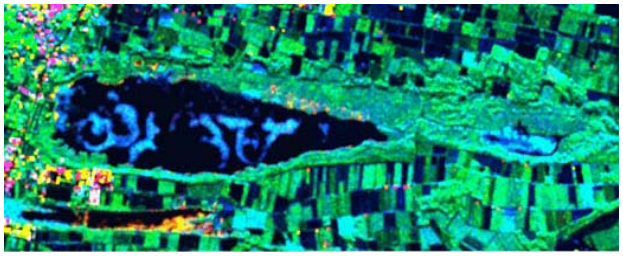

(e) X-band decomposed image in 2004.8

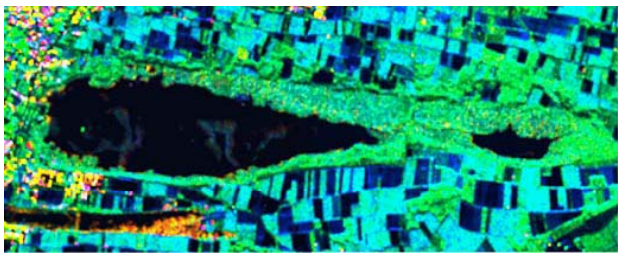

(f) X-band decomposed image in 2004.11

Fig.3 Color-coded decomposed images of SAKATA area: Ps (Blue), Pd (Red), Pv (Green)

The scattering powers are color-coded as Green for Pv (volume scattering), Red for Pd (double bounce scattering), and Blue for Ps (surface scattering). Since Pc was small enough compared to other powers, it was omitted here to illustrate.

As can be seen in Fig.3, there are significant changes in the scattering mechanisms according to season. Both the L- and X-band images are dark in February, because the area is covered with snow and snow act as electromagnetic absorber. The red area in the upper left corner of the image is caused by double bounce reflections from houses. There are several red spots in images in February. Red spots are caused by man-made structures.

In the middest of summer, vegetations are rich in the field generating Ps and Pd larger. Of special interest is the middle of the lake. The L-band image yielded Red (Pd), while X-band image produced Blue (Ps). The reason of the difference is the scattering mechanism in frequency band within the Lotus and Reed. The vertical stem of Reed and the water surface constitute right angle structure in the small lake, causing double bounce reflection in the L-band.

On the other hand, the vegetation structures cannot act as corner reflector for the X-band because of the shorter wavelength and attenuation within the structures. The X-band wave cannot penetrate into the vegetation.

In addition, the Ps (Blue) in the lake in the X-band image (e) is caused only by Lotus. Since Lotus has thick broad-leaves, the surface scattering dominates in the X-band.

In November, some crops are harvested and some are ripening. This situation caused various patterns near by the lake in the L- and X-band images. Blue color (Ps) is caused by rough surface scattering in the crop field after harvesting.

In order to examine the image analysis quantitatively, we took a box region as indicated in Fig.2 (a) where Reed and other vegetations resided and we calculated out the distribution of each scattering power within the spot in the L-band. The result is shown in Fig.4.

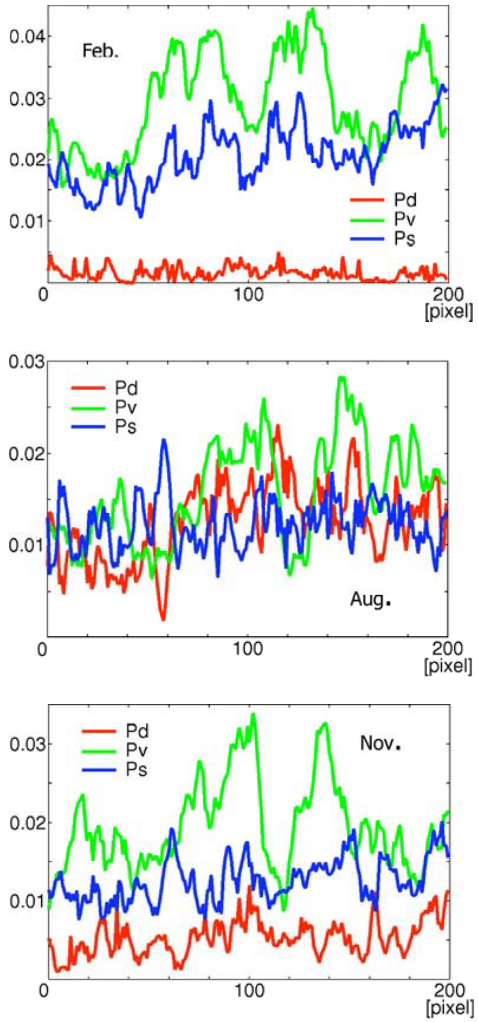

Fig. 4 Contribution of 3 scattering powers

From the inspection of Fig.4, it is seen that ratio of Pd agrees with the growing stage of Reed. In Feb., there is no Pd, while in summer, Pd grows up, and in November, Pd decreases again. In the August, the contribution of each scattering power is almost the same. This would cause polarimetric entropy very high, showing highly complex scattering nature. The contribution of decomposed power Pd may be used for monitoring the status of bushes, reeds around the wet land.

Finally, the total power in the L-band in August, together with a transect is shown in Fig.5 (a). Figure 5 (b) is illustrated for checking the seasonal change of total scattering powers along the transect. Since the transect is drawn including soil, water, ice in winter, Lotus, water and soil, the variation in season can be recognized. Lines in Fig.5 (b) reflect the status of each target and the boundary.

5. CONCLUDING REMARKS

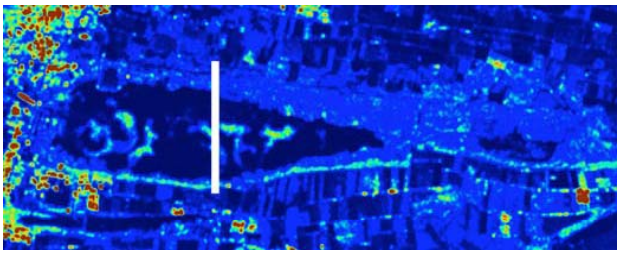

Fig.5 (a) L-band total scattering power in August

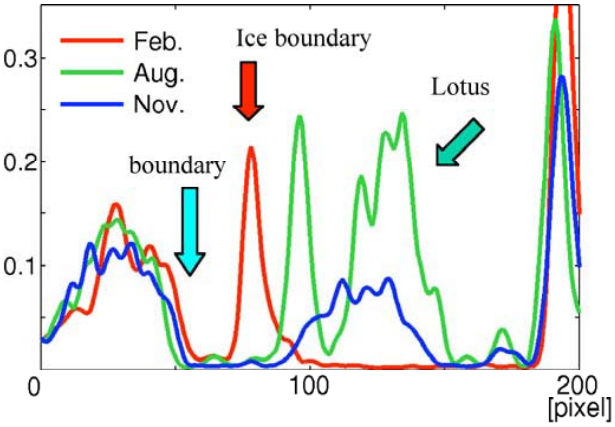

Fig.5 (b) Total scattering power along a transect Fig.5(a)

A polarimteric decomposition of scattering power is applied to monitor seasonal change of wetland area. It is found that the decomposed image clearly exhibits seasonal change of the area indicating that the double bounce power bears the information of growing stage of vegetation. Since the decomposition scheme produces three or four components, it can be employed as one of monitoring tools for environmental remote sensing.

ACKNOWLEDGEMENT

The authors are grateful for NiCT and JAXA, Japan, for providing Pi-SAR data sets. This work in part was supported by a Grant-in-Aid for Scientific Research, JSPS, Japan.

REFERENCES

[1] Y. Yamaguchi, Y. Yajima, and H. Yamada, "Four-component decomposition of POLSAR image based on coherency matrix", *IEEE GRSL*, vol. 3, no.3, pp.292-296, July 2006.

[2] Y. Yamaguchi, T. Moriyama, M. Ishido, and H. Yamada, "Four-component scattering model for polarimetric SAR image decomposition," *IEEE TGRS*, vol.43, no.8, pp.1699-1706, Aug. 2005

[3] A. Freeman and S. L. Durden, "A three-component scattering model for polarimetric SAR data," *IEEE TGRS*, vol.36, no.3, pp.936-973, May 1998.

[4] Y. Yajima, Y. Yamaguchi, R. Sato, and H. Yamada, "POLSAR image analysis of Sakata using four-component scattering model," *National Convention Record of IEICE*, B-2-19, Sept. 2005.